Estimation of Damage Areas due to the 2010 Maule, Chile Earthquake Tsunami Using ASTER/DEM and ALOS/PALSAR Images

Masashi Matsuoka
Senior Research Scientist
AIST
Tsukuba, Japan
m.matsuoka@aist.go.jp

Masashi Matsuoka, born in 1967, received his BS degree in architectural engineering from Muroran Institute of Technology in 1990. In 1992 and 1996, respectively, he received his MS and PhD degrees in engineering of built environment, both from Tokyo Institute of Technology. He was with Tokyo Institute of Technology, RESTEC, and NIED prior to joining AIST.

Shunichi Koshimura
Assoc. Professor
Tohoku University
Sendai, Japan
koshimura@tsunami2.civil.tohoku.ac.jp

Shunichi Koshimura, born in 1972, received Ph.D. degree from Tohoku University in 2000, and he started his dual appointment as a JSPS research fellow and a postdoctoral researcher in Pacific Marine Environmental Laboratory, NOAA. In 2005, he joined Tohoku University, as an associate professor.

Summary

We propose using satellite remote sensing technology with a modified damage detection model based on the regression discriminant function for severe building damage ratios as a method to quickly estimate damaged areas due to tsunamis anywhere in the world. The model was developed using a data set from JERS-1/SAR images of the aftermath of the 1995 Kobe earthquake and its detailed ground-truth data, and was applied to ALOS/PALSAR images acquired before and after the 2010 Maule, Chile earthquake tsunami. The modified model considers the backscattering characteristics of tsunami-damaged buildings and scattered debris in the affected areas and the ground elevation as measured by Terra/ASTER stereoscopic observations. The accuracy of the proposed damage estimation model is examined by comparing it with the results of field survey data and interpretation of high-resolution satellite optical images taken after the event.

Keywords: synthetic aperture radar; DEM; tsunami damage; ALOS/PALSAR; Terra/ASTER; GEO Grid.

1. Introduction

It is quite difficult to get an accurate overview of large-scale natural disasters such as earthquakes, tsunamis, windstorms, floods, and landslides. We expect damage assessment to take longer the greater the extent of the damaged area. In order to properly respond to a disaster, observations of the damaged area by helicopters, airplanes, and satellites may be able to fill the time lag of field damage assessment. In particular, remote sensing by satellites can provide observation of a wide area with a single image and it may be possible to use this technology to improve the estimation accuracy for large-scale damage [1, 2]. For assessing affected areas due to tsunamis, landforms are a significant factor in determining the extent of tsunami run-up [3]. Generally, global-based digital elevation models (DEMs), which are generated from stereoscopic pairs of optical sensor images like SPOT DEM [4] and ASTER (Advanced Spaceborne Thermal Emission and Reflection Radiometer) GDEM [5], or using interferometric approaches using Synthetic Aperture Radar (SAR) images like Shuttle Radar Topography Mission (SRTM) [6], can be employed to map the susceptibility of areas to large-scale tsunami inundation. In order to access higher resolution DEMs, it is possible to use the ASTER on-demand processing service and data from the “GEO (Global Earth Observation) Grid” system administered by the National Institute of Advanced Industrial Science and Technology (AIST), Japan [7]. The GEO Grid also contributes by providing large-scale archived data related to earth observation including not only ASTER but also Phased Array L-band

Synthetic Aperture Radar (PALSAR) images.

Among the remote sensors, SAR is remarkable for its ability to record the physical value of the Earth's surface [8]. Unlike passive optical sensors, SAR enables observation of surface conditions day or night, even through clouds. SAR interferometric analyses using phase information have successfully provided quantification of relative ground displacement levels due to natural disasters [9]. More importantly, intensity information obtained from SAR represents a physical value (backscattering coefficient) that is strongly dependent on the roughness of the ground surface and the dielectric constant, but independent of observation conditions such as the baseline length of satellite orbits [10]. Based on this idea, we have developed models for satellite C- and L-band SAR data to map building damage areas by clarifying the relationship between the change in the backscattering coefficient before and after earthquakes, and building damage assessment based on detailed field investigations following the 1995 Kobe earthquake [11, 12].

In this paper, we introduce an example application, mapping tsunami-induced damage due to the 2010 Maule, Chile earthquake using the ASTER DEM and PALSAR images on a GEO Grid data set. We evaluate tsunami inundation susceptibility based on a DEM derived from pre-tsunami ASTER images. PALSAR is used for post-event assessment. We examine the backscattering characteristics of damaged areas in the PALSAR images taken before and after the tsunami and then apply a modified model based on Matsuoka and Nojima [12] in order to extract severely damage areas. The results of the damage estimation are examined by comparing the results of field survey data and interpretation of high-resolution satellite optical images taken after the event.

2. ASTER DEM and Inundation Susceptibility Map

2.1 GEO Grid and ASTER DEM

The GEO Grid system aims at providing an e-infrastructure and large-scale archived data related to earth observation to understand our Earth more precisely and with more insight, as well as being faster and easier to access by the worldwide earth sciences community [13]. One of the most potentially useful archives in GEO Grid is more than 1.8 million ASTER scenes from the Terra earth-observation mission satellite compiled since its launch in 1999. ASTER can cover a wide spectral region covering the visible to thermal ranges with 14 spectral bands. It has three bands in the visible and near-infrared (VNIR) range, six bands in the shortwave infrared (SWIR) range, and five bands in the thermal infrared (TIR) range with 15, 30, and 90 m ground resolutions [14]. The ASTER instrument also has an along-track stereoscopic capability using two telescopes in a near-infrared band, one for nadir-viewing and another for backward-viewing, with a base-to-height ratio of 0.6 [15]. The DEM, whose spatial resolution is 15 m, can be generated by this function without any ground control points (GCPs). The standard deviations of original geolocation accuracy are better than 20 m in the horizontal plane and 10 m along the vertical axis [15].

The GEO Grid system provides several useful options in creating higher quality DEMs and in making them useful in practice [7]. One of the options is geometric correction based on a reference DEM. It performs a geolocation correction of the DEM by calculating the horizontal and vertical offsets between the ASTER DEM and a reference DEM. The relative geolocation accuracy is examined by template matching in the horizontal plane and vertical differences from the reference DEM in a flat area. When using SRTM as the reference DEM, the standard deviation of the geolocation accuracy improves to less than 7.5 m horizontally and 3.3 m vertically [16].

2.2 The 2010 Chile earthquake tsunami and inundation susceptibility

A moment magnitude 8.8 earthquake struck the central region of Chile on February 27, 2010. The earthquake produced a tsunami that caused major damage in locations spanning over 500 km of coastline, from Tirúa to Pichilemu. Coastal locations were affected by both ground shaking and the tsunami. As of May 2010, 521 people had died and 56 persons were still missing. The earthquake and tsunami destroyed over 81,000 houses, and another 109,000 were severely damaged [17].

In order to understand the topographic characteristics of affected areas, we searched and selected cloudless ASTER images of the Biobio region from the GEO Grid ASTER archives, then generated orthorectified images and DEMs with 15 m ground resolution. Fig. 1 show the false color

composite images and DEM in the areas of Concepcion (Feb. 5, 2001). We found that there are cities located on small plains along the coast with several valley bottom lowlands. According to the tsunami surveys [18] and simulation [19], the maximum expected tsunami height is approximately 25 m above sea level. So, as a first stage estimate, areas where the elevation is lower than 25 m are considered to be susceptible to tsunami inundation as shown in Fig. 2. According to this simple estimation, most of the major cities in the region are at risk of inundation.

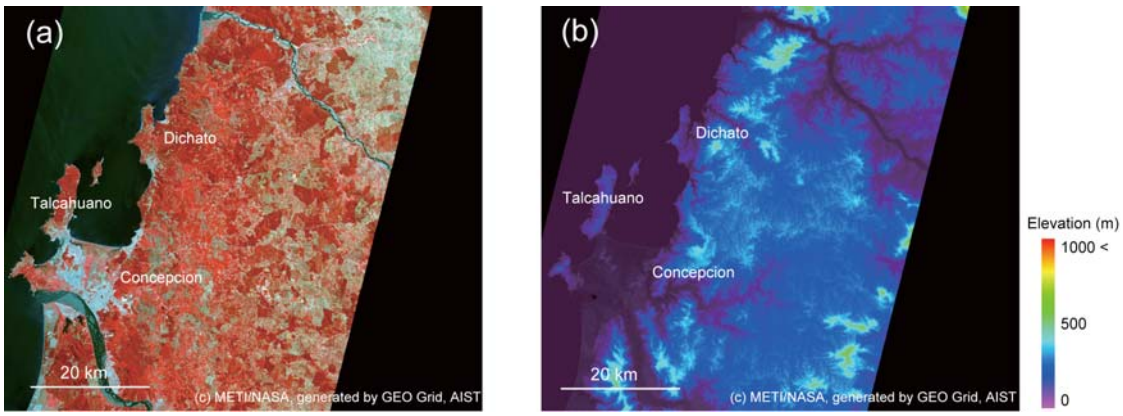

Fig. 1: (a) ASTER false color composite and (b) DEM images of the Concepcion, Talcahuano, and Dichat areas. Image taken February 5, 2001.

3. PALSAR Images and Damage Detection

3.1 Backscattering characteristics in damaged area

Two weeks after the event, the PALSAR unit on the Advanced Land Observing Satellite (ALOS) observed the Concepcion area in fine-beam-mode, which captures the earth surface with approximately 10-meter resolution. Fig. 3 shows the pre- and post-tsunami images by PALSAR. The images acquired on March 11, 2009 was used for the data prior to the event. These PALSAR data are also stored in the GEO Grid archives and the image processing, including orthorectification, was carried out using the GAMMA Software in the system [20].

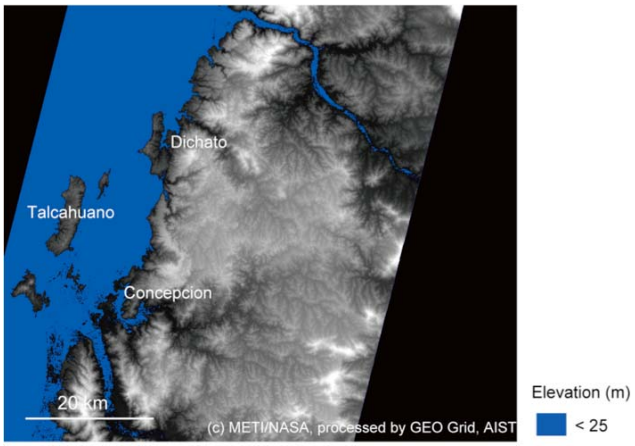

Fig. 2: Map of estimated susceptibility to tsunami inundation (blue region) in Concepcion area based on the ASTER DEM.

Fig. 4 shows zoomed-in pre- and post-tsunami PALSAR images used to examine the backscattering characteristics of tsunami damage in typical areas in Dichato city, where totally collapsed buildings are identified in the optical sensor images on Google Earth. Typically, man-made structures show comparatively high reflection due to the cardinal effect of structures and the ground. Open spaces or damaged buildings have comparatively low reflectance because microwaves are scattered in different directions. Buildings may be reduced to debris by earthquake ground motion, and in some cases, the debris of buildings may be removed, leaving the ground exposed. Thus, the backscattering coefficient determined after collapse is likely to be lower than that obtained prior to the event [11, 12]. However, the reverse occurred in the damaged areas marked by dotted red circles in fig. 4. To explain these anomalies in the PALSAR images, several factors need to be considered such as the relationship among the illumination direction of microwaves transmitted from the satellite, the longitudinal direction of buildings, the built-up density of buildings, and changes of earth surface materials. For Dichato city, it seems that scattered debris from collapsed buildings,

visible in open spaces such as roads and bare ground in the post-tsunami image, shows brighter reflections than in the pre-tsunami image. This characteristic that affects the backscattering echo was identified in the tsunami-affected areas in the PALSAR images.

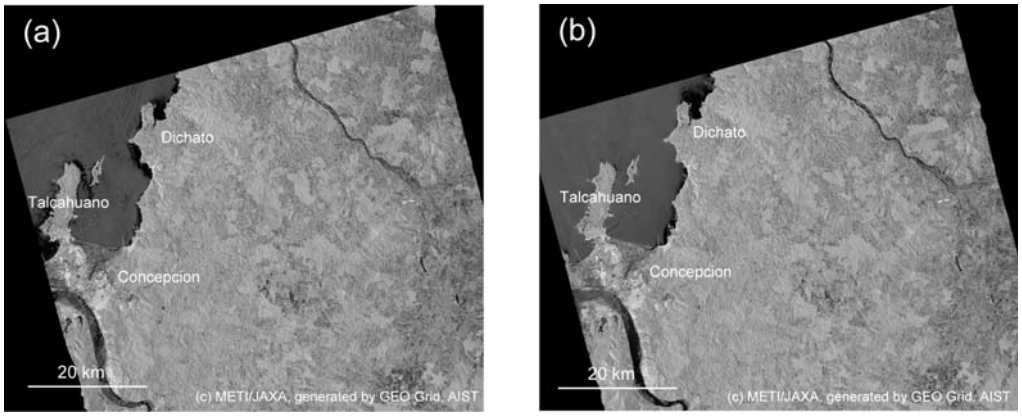

Fig. 3: PALSAR images of the Concepcion, Talcahuano, and Dichato areas before and after the 2010 Maule, Chile earthquake tsunami. (a) Image taken on Mar. 11, 2009. (b) Image taken on Mar. 14, 2010.

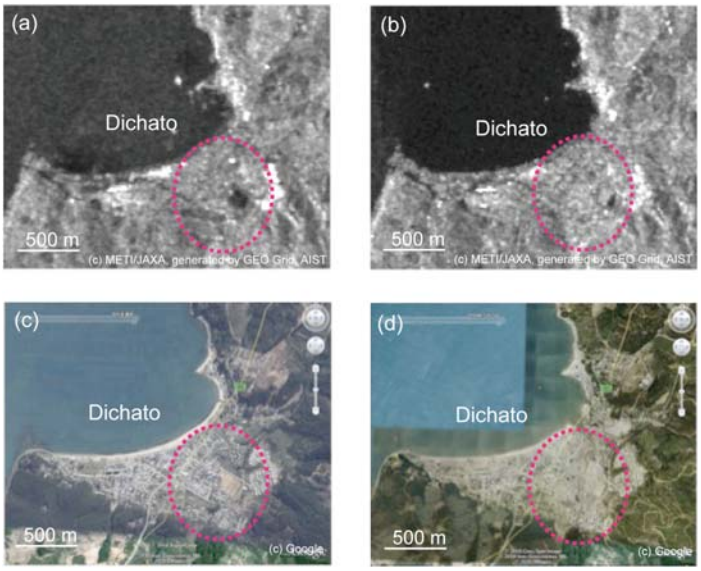

Fig. 4: PALSAR images of Dichato in comparison with optical sensor images on Google Earth before and after the 2010 Maule, Chile earthquake tsunami. (a) Pre-tsunami PALSAR image. (b) Post-tsunami PALSAR image. (c) Pre-tsunami optical image. (d) Post-tsunami optical image.

3.2 Damage detection method

Following Matsuoka and Nojima (2010), the regression discriminant function for building damage was calculated from two characteristic values, the correlation coefficient and the difference in backscattering coefficient for pre- and post-event SAR images [12]. First, following accurate positioning of the two SAR images, a speckle noise filter with a 21×21 pixel window [21] was applied to each image. The difference value, d, is calculated by subtracting the average value of the backscattering coefficient within a 13×13 pixel window in the pre-event image from the post-event image (after – before). The correlation coefficient, r, is also calculated from the same 13×13 pixel window [11]. The result of applying regression discriminant analysis, using the d's and r's from the building damage data set of the 1995 Kobe earthquake, is shown in Equation 1.

$$Z_{Rj} = -1.277d - 2.729r \qquad (1)$$

Here, Z_{Rj} represents the discriminant score from the SAR images. The pixels whose value Z_{Rj} is positive are interpreted as suffering severe damage. Because both coefficients are negative, higher and negative d's or smaller r's produce larger Z_{Rj} values.

However, in the tsunami damage areas in the PALSAR images in the above-mentioned examination, the backscattered echoes were stronger in the post-tsunami image. In order to detect such damaged areas using an image analysis, we need to consider cases where the reverse occurs. Therefore we calculated the absolute value of the difference in backscattering coefficient, $|d|$, and which changed the coefficient of the difference to positive values as shown in Equation 2.

$$Z_{Rj}' = 1.277|d| - 2.729r \quad (2)$$

Here, Z_{Rj}' represents the modified discriminant score. Using this formula, the pixels whose value Z_{Rj}' is positive might be assigned as areas damaged not only by earthquakes but also by tsunamis.

3.3 Damage detection for the 2010 Chile earthquake tsunami

Using the procedure described above and the PALSAR images of the 2010 Chile earthquake tsunami, we calculated discriminant scores Z_{Rj}' in the areas shown to be vulnerable on the inundation susceptibility maps (Fig. 2) and estimated the tsunami damage distribution. The results are shown in fig. 5. The sections on the sea are masked, but areas where the river could not be masked have large Z_{Rj}' values because of surface changes caused by the flow of water. The wetlands near Talcahuano, where the Z_{Rj}' values are large, seem to be affected by the tsunami.

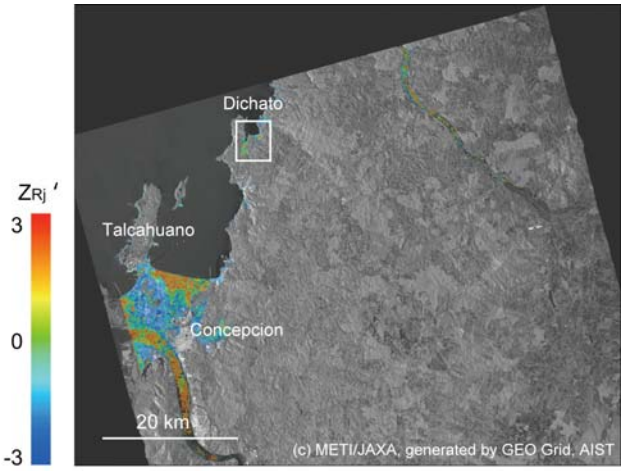

Fig. 5: Distribution of Z_{Rj}' obtained by ALSAR images.

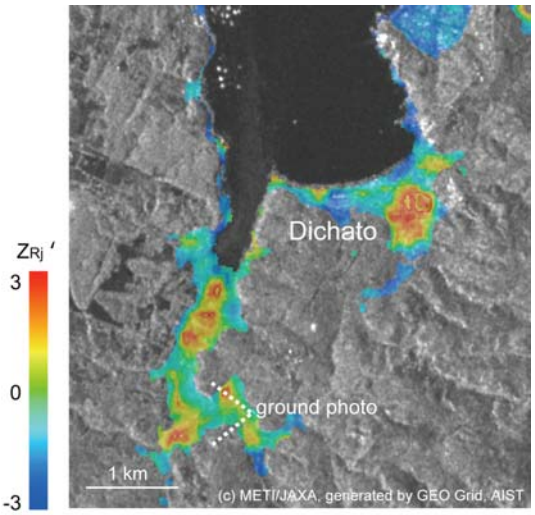

Fig. 6: Distribution of Z_{Rj}' in a close-up of the Dichato area.

Fig. 6 shows a close-up Z_{Rj}' image of the Dichato area. This agrees well with the post-tsunami optical image, Fig. 4(d). Fig. 7 shows a ground photo near Dichato city taken on April 24, 2010. The viewing area of the ground photo (dotted lines) is shown in Fig. 6 to correspond to areas with large Z_{Rj}'. Though the location is far from the coastline, we found that the tsunami surged to that point.

Fig. 7: Ground photo whose location is drawn in fig. 6, taken on April 24, 2010.

4. Conclusions

This paper proposed a scheme to detect damage due to tsunamis using an ASTER DEM and PALSAR images stored and processed on the GEO Grid system developed by AIST. First, maps of susceptibility to tsunami inundation were created by threshold classification using the ground elevation from the ASTER DEM. Second, a modified damage detection model, based originally based on data from the 1995 Kobe earthquake, was proposed, making use of the phenomena that backscattering intensity increases in debris-strewn areas. We then examined the relationship between the backscattering echo in PALSAR images and the areas affected by tsunami following the 2010 Maule, Chile earthquake. Finally, we applied this model to PALSAR images and compared the results with optical sensor images and field survey data with ground photos. For

estimations of tsunami damage, the function for the Kobe earthquake was used but it would be preferable for a suitable fragility function for tsunami damage to be developed in order to further increase the accuracy of damage estimation.

Acknowledgements

The ASTER and PALSAR data are the property of METI/NASA and METI/JAXA, respectively. We received grants for part of the research from the "Development of real-time tsunami damage detection technology for expeditious disaster response by Japan and ASEAN countries (Project ID: 08E52010a)", the NEDO Industrial Technology Research Grant Program, the "Enhancement of Earthquake and Tsunami Disaster Mitigation Technology in Peru", JST-JICA's Science and Technology Research Partnership for Sustainable Development (SATREPS), and a grant-in-aid for scientific research (Research No. 21310119). We would like to express our gratitude.

References

[1] EGUCHI, R.T., HUYCK, C.K., ADAMS, B.J., MANSOURI, B., HOUSHMAND, B., and SHINOZUKA, M., "Resilient disaster response: Using remote sensing technologies for post-earthquake damage detection," *Research Progress and Accomplishments 2001-2003*, MCEER, 2003, pp.125–137.

[2] SAITO, K., SPENCE, R.J.S., GOING, C., and MARKUS, M., "Using high-resolution satellite images for post-earthquake building damage assessment: A study following the 26 January 2001 Gujarat Earthquake," *Earthquake Spectra*, Vol.20, No.1, 2004, pp.145–169.

[3] KOUCHI, K. and YAMAZAKI, F., "Characteristics of tsunami-affected areas in moderate-resolution satellite images," *IEEE Trans. Geosci. Remote Sens.*, Vol.45, No.6, 2007, pp.1650-1657.

[4] SPOTIMAGE, *SPOT DEM Precision Product description ver.1.0*, available online: http://www.spotimage.com/automne_modules_files/standard/public/p807_97114bc824a947c5af8914cdf4b351edSPOT__DEM_Precision_Product_description_V1.0.pdf (access on 31 Aug. 2010).

[5] EARTH REMOTE SENSING DATA ANALYSIS CENTER, *ASTER GDEM*, available online: http://www.gdem.aster.ersdac.or.jp/ (access on 31 Aug. 2010).

[6] FARR, T., and KOBRICK, M., "The Shuttle Radar Topography Mission produces a wealth of data," *Amer. Geophys*. Union EOS, Vol. 81, 2000, pp.583-585.

[7] KODAMA, S., YAMAMOTO H., YAMAMOTO, N., KAMEI, A., NAKAMURA, R., IWAO, K., and TSUCHIDA, S., "ASTER digital elevation model and orthorectified images generated on the GEO Grid," *Proc. IEEE IGRASS 2010*, CD-ROM, 2010, 4p.

[8] HENDERSON, F.M., and LEWIS, A.J., *Principles and Applications of Imaging Radar*, Manual of Remote Sensing, 2, John Wiley & Sons, Inc., New York, 1998.

[9] MASSONNET, D., ROSSI, M., CARMONA, C., ADRAGNA, F., PELTZER, G., FIEGL, K., and RABAUTE, T., "The displacement field of the Landars earthquake mapped by radar interferometry," *Nature*, No.364, 1993, pp.138-142.

[10] YONEZAWA, C., and TAKEUCHI, S., "Decorrelation of SAR data by urban damages caused by the 1995 Hyogoken-Nanbu earthquake," *International Journal of Remote Sensing*, Vol.22, No.8, 2001, pp.1585–1600.

[11] MATSUOKA, M., and YAMAZAKI, F., "Use of Satellite SAR intensity imagery for detecting building areas damaged due to earthquakes," *Earthquake Spectra*, Vol.20, No.3, 2004, pp.975–994.

[12] MATSUOKA M., and NOJIMA, N., "Estimation of building damage ratio due to earthquakes using satellite L-band SAR imagery," *Proc. 7th International Workshop on Remote Sensing and Disaster Response*, 2009.

[13] SEKIGUCHI, S., TANAKA, Y., KOJIMA, I., YAMAMOTO, N., YOKOYAMA, S., TANIMURA, Y., NAKAMURA, R., IWAO, K., and TSUCHIDA, S., "Design principles and

IT overviews of the GEO Grid," *IEEE Systems Journal*, Vol.2, No.3, 2008, pp.374-389.

[14] YAMAGUCHI, Y., KAHLE, A.B., TSU, H., KAWAKAMI, T., and PNIEL, M., "Overview of Advanced Spaceborne Thermal Emission and Reflection Radiometer (ASTER)," *IEEE Trans. Geosci. Remote Sens.*, Vol.36, No.4, 1998, pp.1062-1071.

[15] FUJISADA, H., BAILEY, G.B., KELLY, G.G., HARA, S., and ABRAMS, M.J., "ASTER DEM performance," *IEEE Trans. Geosci. Remote Sens.*, Vol.43, No.12, 2005, pp.2707-2714.

[16] KODAMA, S., ARIOKA, M., MIO, A., NAKAMURA, R., and IWAO, K., "Geometric accuracy of ASTER DEM," *Proc. the 43rd Autumn Conference of the Remote Sensing Society of Japan*, 2007, pp.241-242 (in Japanese).

[17] EARTHQUAKE ENGINEERING RESEARCH INSTITUTE, *The Mw8.8 Chile Earthquake of February 27, 2010*, EERI Special Earthquake Report, 2010.

[18] NOAA NATIONAL GEOPHYSICAL DATA CENTER, *NOAA/WDC Historical Tsunami Database*, available online: http://www.ngdc.noaa.gov/hazard/tsu_db.shtml (access on 1 Aug. 2010).

[19] KOSHIMURA, S., TAKASHIMA, M., SUZUKI, S., HAYASHI, H., IMAMURA, F., and KAWATA, Y., "Estimation of the possible tsunami disaster potential within the Indian Ocean," *Annual Journal of Coastal Engineering*, Japan Society of Civil Engineers, Vol.52, 2005, pp.1416-1420 (in Japanese).

[20] TAKEYAMA, Y., KODAMA, S., NAKAMURA, K., MATSUOKA, M., and YAMAMOTO, N., "Development of ALOS/PALSAR data on-demand processing and providing system on GEO Grid," *Proc. IEEE IGRASS 2010*, CD-ROM, 2010, 3p.

[21] LEE, J.S., "Digital image enhancement and noise filtering by use of local statistics," *IEEE Trans. Pattern Analysis and Machine Intelligence*, No.2, 1980, pp.165-168.